The Astrophysical Journal, 953:141 (10pp), 2023 August 20 https://doi.org/10.3847/1538-4357/ace1eb

On the Tidal Capture of White Dwarfs by Intermediate-mass Black Holes in Dense Stellar Environments

Claire S. Ye[1], Giacomo Fragione[2,3], and Rosalba Perna[4,5]
[1] Canadian Institute for Theoretical Astrophysics, University of Toronto, 60 St. George Street, Toronto, Ontario M5S 3H8, Canada; claireshiye@cita.utoronto.ca, s.yephysics@gmail.com
[2] Department of Physics & Astronomy, Northwestern University, Evanston, IL 60208, USA
[3] Center for Interdisciplinary Exploration & Research in Astrophysics (CIERA), Northwestern University, Evanston, IL 60208, USA
[4] Department of Physics and Astronomy, Stony Brook University, Stony Brook, NY 11794, USA
[5] Center for Computational Astrophysics, Flatiron Institute, 162 5th Avenue, New York, NY 10010, USA
Received 2023 March 10; revised 2023 May 21; accepted 2023 June 15; published 2023 August 11

Abstract

Intermediate-mass black holes (IMBHs) are the missing link between stellar-mass and supermassive black holes, widely believed to reside in at least some dense star clusters, but not yet observed directly. Tidal disruptions of white dwarfs (WDs) are luminous only for black holes less massive than $\sim 10^5\,M_\odot$, therefore providing a unique smoking gun that could finally prove the existence of IMBHs beyond any reasonable doubt. Here, we investigate the tidal captures of WDs by IMBHs in dense star clusters, and estimate upper limits to the capture rates of $\sim 1\,\mathrm{Myr}^{-1}$ for galactic nuclei and $\sim 0.01\,\mathrm{Myr}^{-1}$ for globular clusters. Following the capture, the WD inspirals onto the IMBH, producing gravitational waves detectable out to ~ 100 Mpc by LISA for $\sim 10^4\,M_\odot$ IMBHs. The subsequent tidal stripping/disruption of the WD can also release bright X-ray and gamma-ray emission with luminosities of at least $\gtrsim 10^{40}\,\mathrm{erg\,s}^{-1}$, detectable by Chandra, Swift, and upcoming telescopes, such as the Einstein Probe.

Unified Astronomy Thesaurus concepts: Intermediate-mass black holes (816); Star clusters (1567); Tidal interaction (1699); White dwarf stars (1799)

1. Introduction

Intermediate-mass black holes (IMBHs) are some of the most mysterious objects in the universe. They are often introduced as the black holes (BHs) occupying the mass range between stellar-mass BHs ($\sim 10\,M_\odot$) and supermassive black holes (SMBHs; 10^6–$10^{10}\,M_\odot$). IMBHs may play a crucial role in cosmology and galaxy formation, as they could act as building blocks of SMBHs that are observed at the centers of most galaxies (see, e.g., Greene et al. 2020 and references therein). Understanding how IMBH masses are related to their environments (e.g., velocity dispersion) may also provide unique insights into the dynamical evolution of dense star clusters (e.g., Miller & Hamilton 2002; Portegies Zwart & McMillan 2002; Gürkan et al. 2004; Šubr et al. 2019). Furthermore, the inspirals of stellar compact remnants into an IMBH could provide an extraordinarily powerful tool for testing general relativity in the strong-field regime (e.g., Miller 2002). Despite these rich physical applications, the existence of IMBHs has long been debated and very little is known about their origin and evolution. Only recently was their existence confirmed, when a $150\,M_\odot$ binary BH merger was detected by LIGO/Virgo (Abbott et al. 2020).

IMBHs are most likely produced in dense stellar environments, such as globular clusters (GCs) and galactic nuclei. They could form through collisional runaways of massive stars (e.g., Portegies Zwart & McMillan 2002; Giersz et al. 2015; Kremer et al. 2020; González et al. 2021) or through repeated mergers of stellar-mass BHs (e.g., Miller & Hamilton 2002; Antonini et al. 2019; Fragione et al. 2022; Mapelli et al. 2022). Here, IMBHs can also have frequent dynamical encounters with stars and compact objects. For example, during these interactions, it is very likely that the IMBHs will quickly form binaries with other compact objects through exchange encounters. The subsequent intermediate-mass inspirals of the stellar remnants into the IMBHs can produce gravitational wave (GW) sources detectable by LISA and ground-based telescopes such as the Einstein Telescope (Jani et al. 2020; Fragione & Loeb 2023).

IMBHs are also uniquely suited to tidally disrupting white dwarfs (WDs). The tidal disruption radius of a WD is outside the event horizon of an IMBH; on the other hand, the tidal disruption radius of a WD is inside the event horizon of an SMBH, so no electromagnetic waves can be observed, and a stellar-mass BH will enter a WD instead of disrupting it during close encounters (Luminet & Pichon 1989; Maguire et al. 2020). Since WD tidal disruptions are a smoking gun for revealing IMBHs, they have been under intense scrutiny (e.g., Baumgardt et al. 2004; Rosswog et al. 2008a, 2008b, 2009; Sesana et al. 2008; Zalamea et al. 2010; Clausen & Eracleous 2011; Haas et al. 2012; MacLeod et al. 2014, 2016a, 2016b; Tanikawa et al. 2017, 2022; Fragione et al. 2018b; Anninos et al. 2018; Fragione & Leigh 2018; Kawana et al. 2018; Toscani et al. 2020; Chen et al. 2023).

Despite the wealth of studies on WD tidal disruptions, little attention has been devoted to computing the tidal capture rates of WDs, with the possible exception of Ivanov & Papaloizou (2007). In this study, we explore in detail the characteristics of IMBH–WD tidal interactions in both galactic nuclei and GCs. During close encounters, the tidal force exerted by an IMBH can induce oscillations within the WD, which can then lead to the formation of an IMBH–WD binary. This mechanism for capturing WDs is different from binary splitting according to the Hills mechanism which requires a binary or the scattering

of WDs into the loss cone, and thus provides an additional channel for IMBH–WD binary formation (Hills 1988). These captured binaries are prime sources of low-frequency gravitational radiation during their inspiral and will provide key GW sources for future space detectors such as LISA (e.g., Amaro-Seoane et al. 2007, 2017; Fragione et al. 2018a). Subsequent tidal stripping/disruption of the WD can be observed by ongoing and future time-domain surveys (e.g., Maguire et al. 2020, for a review). These multiwavelength detections will provide definitive evidence for the existence of IMBHs.

Our paper is organized as follows. In Section 2, we describe the analytical methods used to calculate the WD oscillation energy during close passages to the IMBHs. In Section 3, we discuss the WD tidal capture rates in different dense star clusters, while we show the potential multiwavelength signals from gravitational radiation and WD stripping/disruption in Section 4. Lastly, we discuss the uncertainties and conclude in Section 5.

2. Tidal Captures of White Dwarfs

In this section, we describe the methods used for estimating the tidal capture rates of WDs by an IMBH in galactic nuclei and GCs.

Throughout this study, we fix the mass of the WDs to be $0.6\,M_\odot$ and adopt Equation (91) in Hurley et al. (2000) for the radius of a WD. These low-mass WDs are well represented by an $n = 1.5$ polytrope (Shapiro & Teukolsky 1983). Following Fabian et al. (1975), Press & Teukolsky (1977), and Lee & Ostriker (1986), we estimate the amount of oscillation energy deposited into a WD that is passing at a distance R_p from an IMBH as

$$\Delta E_{\rm osc} = \frac{GM_{\rm WD}^2}{R_{\rm WD}}\left(\frac{M_{\rm IMBH}}{M_{\rm WD}}\right)^2\sum_{l=2}^{\infty}\left(\frac{R_{\rm WD}}{R_p}\right)^{2l+2}T_l(\eta), \quad (1)$$

where $M_{\rm WD}$ and $R_{\rm WD}$ are the mass and radius of the WD, respectively, T_l is a dimensionless function measuring the contributions from different harmonic modes l (we include the quadruple and octupole terms), and η is the duration of the periastron passage,

$$\eta = \left(\frac{M_{\rm WD}}{M_{\rm WD}+M_{\rm IMBH}}\right)^{1/2}\left(\frac{R_p}{R_{\rm WD}}\right)^{3/2}. \quad (2)$$

This linear energy approximation agrees well with more detailed energy calculations except at small R_p (e.g., Cheng & Evans 2013, and in particular their Figure 9).

The maximum tidal capture radius, $R_{\rm cap}$, is obtained when the total initial kinetic energy of the two interacting objects, $E_{\rm orb} = \frac{1}{2}\mu v_{\rm rel}^2$ ($v_{\rm rel}$ is the relative velocity between the IMBH and WD at infinity), equals $\Delta E_{\rm osc}$, assuming fast dissipation of the oscillation energy.

The effect of an IMBH's tidal force on a WD is stronger the closer the WD is to the IMBH, as can be seen from Equation (1). Figure 1 shows the amount of orbital energy injected into a WD during the first passage of tidal interactions with IMBHs of different masses. For example, for an encounter of a $10^3\,M_\odot$ IMBH with a WD where the pericenter distance is smaller than $\sim 30R_{\rm WD}$, the energy deposited into the WD and subsequently dissipated through its oscillation exceeds the total initial kinetic energy assuming a velocity dispersion of

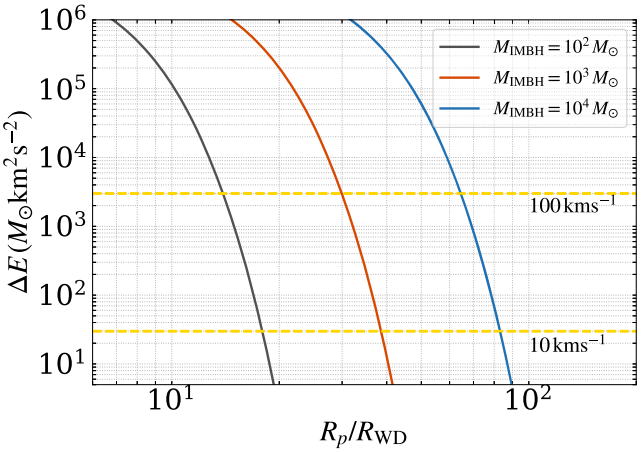

Figure 1. The amount of energy deposited into a WD after one periastron passage as a function of the pericenter distance in units of the WD radius. The two yellow horizontal lines show the total initial kinetic energy of a $10^3\,M_\odot$ IMBH and a $0.6\,M_\odot$ WD with relative velocities at infinity of 10 km s^{-1} and 100 km s^{-1}, respectively. For small pericenter distances, the oscillation energy is larger than the total kinetic energy.

100 km s^{-1}. For lower velocity dispersions, e.g., in GCs where σ_v is $\sim$10 km s^{-1}, the minimum pericenter distance is larger, at $\sim 40R_{\rm WD}$. For all IMBH masses, the maximum capture radii in GCs are about 1.3 times larger than those in galactic nuclei for the velocity dispersions considered in Figure 1.

The capture cross section can then be written as (Quinlan & Shapiro 1987)

$$\sigma_{\rm cap} = \pi R_{\rm cap}^2\left(1 + \frac{2GM_{\rm IMBH}(1+q)}{R_{\rm cap}v_{\rm rel}^2}\right), \quad (3)$$

where $q = M_{\rm WD}/M_{\rm IMBH}$. We adopt in the calculations $v_{\rm rel} \approx \sigma_v$ as typical, where σ_v is the local velocity dispersion, but note that $v_{\rm rel}$ can be up to $2\sigma_v$. Thus, the rates of IMBH–WD tidal captures (per IMBH) can be estimated by the two-body collision rates

$$\Gamma = n\sigma_{\rm cap}\sigma_v, \quad (4)$$

where n is the local WD number density.[6] The timescale for tidal capture is

$$T_{\rm IMBH-WD} = \Gamma^{-1}. \quad (5)$$

At the moment of tidal capture, the semimajor axis of the newly formed IMBH–WD binary, a, can be calculated from its binding energy E_b as

$$a = \frac{GM_{\rm IMBH}M_{\rm WD}}{2|E_b|}, \quad (6)$$

and the eccentricity, e, can then be derived from $R_{\rm cap} = a(1-e)$. For E_b close to zero, the orbit will tend to be parabolic, and a and e will be close to infinity and unity, respectively. To estimate the minimum a and e, we assume that the total initial energy, $E_{\rm orb}$, is zero, and that $E_b = \Delta E_{\rm osc}$ at the WD's tidal disruption radius. We define the tidal disruption

[6] We assume that the loss cone of the IMBH is full and continuously replenished by WDs since the IMBH is moving through the surrounding cusp and the WDs would have enough time to refill the loss cone. If the loss cone becomes empty, fewer capture/disruption events would occur.

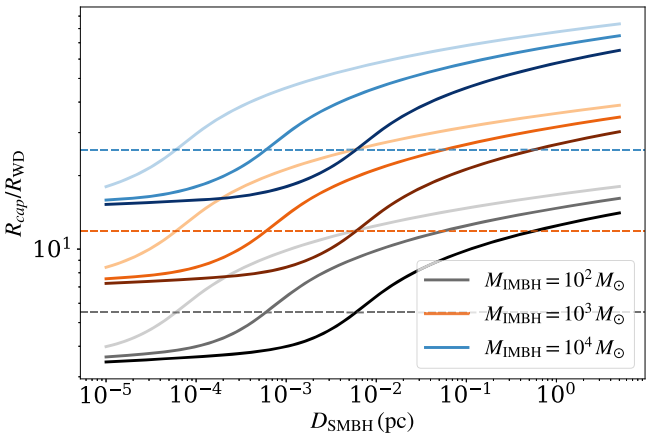

Figure 2. Maximum tidal capture radii for various IMBH and SMBH masses as a function of the distances to the SMBHs in galactic nuclei. The three colors/groups of curves correspond to three IMBH masses of $10^4\,M_\odot$ (blue), $10^3\,M_\odot$ (orange), and $10^2\,M_\odot$ (black) from top to bottom. The curves in each group from top to bottom correspond to increasing SMBH masses of 10^5, 10^6, and $10^7\,M_\odot$, respectively. The horizontal lines show the tidal disruption radii for different IMBH masses.

radius of a WD to be (e.g., Rees 1988)

$$R_t = \left(\frac{M_{\rm IMBH}}{M_{\rm WD}}\right)^{1/3} R_{\rm WD}. \tag{7}$$

The radius of a WD with $M_{\rm WD} = 0.6\,M_\odot$ is about $0.013\,R_\odot$. For IMBHs with masses of 10^2, 10^3, and $10^4\,M_\odot$, the tidal disruption radius of a WD is $5.5R_{\rm WD}$ (3×10^{-4} au), $11.9R_{\rm WD}$ (7×10^{-4} au), and $25.5R_{\rm WD}$ (1.5×10^{-3} au), respectively. The minimum capture semimajor axis and eccentricity, $[a, e]$, are then estimated to be [0.012 au, 0.973], [0.12 au, 0.994], and [1.24 au, 0.999], respectively. Note that these are approximate estimates since the oscillation energy in Equation (1) may have non-negligible contributions from higher-order terms when $R_p \sim R_t$. Both the semimajor axis and eccentricity are larger for binaries captured at larger pericenter distances than the tidal disruption radii (Equation (6)). The maximum capture semimajor axes are about 160, 1641, and 16,456 au for IMBHs with masses of 10^2, 10^3, and $10^4\,M_\odot$, respectively, for captures at about $3R_t$, which is about the maximum tidal capture radius of the WD (Figures 2 and 5). At the same time, the eccentricities tend to be unity (see also Figure 8 below).

3. Rates

In this section, we analyze the capture rates for IMBHs of masses 10^2, 10^3, and $10^4\,M_\odot$ in different dense stellar environments.

3.1. Galactic Nucleus Environments

Here, we consider various galactic nucleus environments hosting SMBHs with masses $M_{\rm SMBH} = 10^5$, 10^6, and $10^7\,M_\odot$. The radius of influence of an SMBH is defined as (Merritt 2013)

$$R_h = \frac{GM_{\rm SMBH}}{v_h^2}, \tag{8}$$

where v_h is the velocity dispersion at R_h. The velocity dispersion is a function of the galactocentric distance r, $\sigma_v \sim (GM_{\rm SMBH}/r)^{1/2}$. Following Tremaine et al. (2002) for the "M–σ" relation, v_h can be expressed as a function of the mass of the SMBH,

$$M_{\rm SMBH} = \gamma v_h^4, \tag{9}$$

and $\gamma \approx 0.0758\,M_\odot\,({\rm km\,s^{-1}})^{-4}$ (Tremaine et al. 2002, Equation (19)). Combining Equations (8) and (9), we can write the radius of influence as

$$R_h = G\gamma^{1/2} M_{\rm SMBH}^{1/2}. \tag{10}$$

We assume power-law number density distributions for the main-sequence stars and WDs surrounding the SMBHs (Gondán et al. 2018, and references therein). The distribution function can be written as

$$n_{\rm WD} = n_{\rm inf}\left(\frac{r}{R_h}\right)^{-\alpha}, \tag{11}$$

where

$$n_{\rm inf} = 1.38\times10^4\sqrt{\frac{10^6\,M_\odot}{M_{\rm SMBH}}}\ {\rm pc}^{-3}. \tag{12}$$

The number density of main-sequence stars is 10 times larger following the same distribution.

In galactic nuclei, a massive binary will gradually inspiral through dynamical friction. Following Gürkan & Rasio (2005, Equation A8), and using the definition that the mass enclosed within R_h equals $2M_{\rm SMBH}$, we can write the dynamical friction time at a distance r as

$$\begin{aligned} T_{\rm df} &= \frac{[1+(1+\beta)(r/R_h)^\beta/2][1+(r/R_h)^\beta]^{0.5}(r/R_h)^{1.5}}{1.5\chi\log\Lambda\beta(r/R_h)^\beta} \\ &\times QT_h \approx 2.67\ {\rm Myr}\left(\frac{Q}{1000}\right) \\ &\times\frac{[1+(1+\beta)(r/R_h)^\beta/2][1+(r/R_h)^\beta]^{0.5}(r/R_h)^{1.5}}{\chi\beta(r/R_h)^\beta}, \end{aligned} \tag{13}$$

where $\beta = 3-\alpha$, $\log\Lambda \sim 5$ is the Coulomb logarithm (McMillan & Portegies Zwart 2003), $Q = M_{\rm SMBH}/M_{\rm IMBH}$, the factor χ can be written as (Binney & Tremaine 2008)

$$\chi = {\rm erf}(X) - \frac{2X}{\sqrt{\pi}}e^{-X^2} \tag{14}$$

with $X = \sqrt{2-\beta}$ (McMillan & Portegies Zwart 2003), and $T_h = R_h/v_h$. The dynamical friction timescale at the radius of influence of a $4\times10^6\ M_\odot$ SMBH is about 2000, 200, and 20 Myr for $M_{\rm IMBH} = 10^2$, 10^3, and $10^4\,M_\odot$, respectively. For these values, the power-law slope of the stellar distribution is assumed to be $\alpha = 1.4$, as derived in numerical calculations of two-body relaxation (Hopman & Alexander 2006).

For shorter distances to the SMBHs, the inspiral of the massive binary is dominated by GW radiation instead, and the GW inspiral timescale is (Peters 1964)

$$\begin{aligned} T_{\rm GW} &= \frac{5}{256}\frac{a_{\rm IMBH}^4 c^5}{G^3 M_{\rm IMBH}^3 Q(1+Q)}(1-e_{\rm IMBH}^2)^{7/2} \\ &\approx 5.84\times10^4\ {\rm Gyr}\ \frac{1}{Q(1+Q)}\left(\frac{a_{\rm IMBH}}{10^{-4}\ {\rm pc}}\right)^4\left(\frac{M_{\rm IMBH}}{10^3\,M_\odot}\right)^{-3}, \end{aligned} \tag{15}$$

where c is the speed of light, and $a_{\rm IMBH}$ and $e_{\rm IMBH}$ are the semimajor axis and eccentricity of the IMBH orbiting the SMBH, respectively. The inspiral timescale due to GW emission is about 10^7, 10^6, and 10^5 Myr for $M_{\rm IMBH}=10^2$, 10^3, and $10^4\,M_\odot$, respectively, assuming the IMBHs are orbiting a $4\times10^6 M_\odot$ SMBH at 10^{-3} times its radius of influence on a circular orbit.

We show in Figure 2 the maximum tidal capture radius in galactic nuclei. The maximum capture radius increases as the distance to the center of galaxies increases or the mass of the central SMBH decreases, which causes the velocity dispersion to decrease. For very small galactocentric distances, the maximum tidal capture radii could be smaller than the tidal disruption radii. At these distances, no tidal capture binaries can form during close encounters between IMBHs and WDs, and the IMBHs will directly disrupt the WDs.

In addition, a WD can only be captured in the galactic nuclei before the IMBHs spiral into the central SMBHs. A successful capture depends on the timescales for dynamical friction (Equation (13)) and GW inspiral (Equation (15)) of the IMBH, and needs to satisfy the condition $T_{\rm IMBH-WD}<\min(T_{\rm df},T_{\rm GW})$. We compare in Figure 3 the typical timescale for an IMBH to capture or tidally disrupt a WD in galactic nuclei with the IMBH's dynamical friction and GW inspiral timescales. The capture/disruption timescale is the shortest for the most massive IMBH orbiting the least massive SMBH. For IMBHs with $M_{\rm IMBH}\gtrsim10^3\,M_\odot$, tidal capture of a WD is possible for relatively flat slopes $\alpha\lesssim1.4$ of stellar number density. Observations and theoretical studies have shown that the power-law slope of the stellar density distribution in the Milky Way nuclear star cluster is $\sim$1.4 (Gallego-Cano et al. 2018, 2020), and may be as low as $\sim$1 for main-sequence stars (Baumgardt et al. 2018; Schödel et al. 2018). Thus the center of our Milky Way can potentially produce tidally captured IMBH–WD binaries. For distances closer to the central SMBH, the WD capture radius is smaller than the tidal disruption radius so a WD cannot be captured (left of the yellow line). In this region when $T_{\rm IMBH-WD}<\min(T_{\rm df},T_{\rm GW})$, an IMBH will directly disrupt a WD during close encounters.

The capture and disruption rates as a function of the distance to the galactic center are shown in Figure 4. The maximum tidal capture rate in a galactic nucleus is $\sim$5 per Myr for an IMBH with $M_{\rm IMBH}=10^4\,M_\odot$ orbiting a $10^5\,M_\odot$ SMBH. For a more typical IMBH mass of $10^3\,M_\odot$ and an SMBH mass of $10^6\,M_\odot$, the tidal capture rate is $\sim$0.02 per Myr. The tidal disruption rate in this case is $\sim$0.1 per Myr.

3.2. Globular Cluster Environments

We assume that GCs can be modeled with a Plummer density profile (Plummer 1911; Binney & Tremaine 2008),

$$\rho(r)=\frac{3M_{\rm cl}}{4\pi b^3}\left(1+\frac{r^2}{b^2}\right)^{-5/2}, \tag{16}$$

where $M_{\rm cl}$ is the total mass of the cluster and b is the Plummer scale length. The half-mass radius of a Plummer sphere is $r_{\rm hm}\approx1.3b$. We adopt a Kroupa initial mass function (Kroupa 2001) between masses $0.08\,M_\odot$ and $150\,M_\odot$ and follow an initial-to-final mass relation from Merritt (2013, Equation (7.22)). At the present day, about 17% of the objects are WDs and we assume that the spatial distribution of the WDs follows the Plummer profile.

The velocity dispersion of a Plummer sphere is

$$\sigma_p^2(r)=\frac{GM_{\rm cl}}{6\sqrt{r^2+b^2}}. \tag{17}$$

Here, we assume that the IMBHs reside at the cluster centers. This is a reasonable assumption given that IMBHs are most likely formed from collisional runaways of stars (e.g., Portegies Zwart & McMillan 2002; Giersz et al. 2015; Kremer et al. 2020; González et al. 2021) or repeated mergers of stellar-mass BHs (e.g., Miller & Hamilton 2002; Antonini et al. 2019; Fragione et al. 2022; Mapelli et al. 2022), which occur around the centers of GCs. Besides, a massive IMBH would quickly mass-segregate back to the cluster center on a timescale of megayears if it is displaced by dynamical encounters. The least massive IMBHs may be more easily displaced or even ejected from their host clusters (e.g., González Prieto et al. 2022), but for this first estimate of the rate we ignore these effects.

Similar to the case of galactic nuclei in the above section, the maximum tidal capture radius increases as the distance to the center of GCs increases or as the total mass of GCs decreases, as is shown in Figure 5 (the increase is slow here). However, the maximum tidal capture radii in this case are always larger than the tidal disruption radii because the velocity dispersion is much smaller in GCs than in galactic nuclei. The tidal capture radius is about $3R_t$ for all IMBH masses.

The capture rates as a function of the distance to the GC centers are shown in Figure 6. For a typical GC with $M_{\rm cl}=2\times10^5\,M_\odot$ hosting a $10^3\,M_\odot$ IMBH at the center, the maximum tidal capture rate is $\sim$0.002 per Myr. The tidal capture rates shown in Figure 6 are also consistent with the rates calculated by Ivanov & Papaloizou (2007). For a Milky Way–like galaxy hosting $\sim$200 GCs, if we assume that all clusters have an IMBH, the optimistic tidal capture rate is a few times 0.1 per Myr per galaxy, roughly comparable to the tidal capture rate from one IMBH in a galactic nucleus.

4. Observational Signatures

We discuss here the multimessenger observational signatures of these IMBH–WD interactions and the detectors that are sensitive to these signals.

4.1. Gravitational Wave Emission

After an IMBH–WD binary is formed, the two objects inspiral via the emission of GW radiation, and the emission will be observable by LISA. To estimate the amount of energy radiated by the binary, we compute the evolution of its semimajor axis and eccentricity by integrating Equation (5.8) from Peters (1964) and stop the evolution when the pericenter distance $R_p=R_t$.

For eccentric binaries, the frequency at peak GW emission is given by Wen (2003):

$$f_{\rm peak}=\frac{\sqrt{G(M_{\rm IMBH}+M_{\rm WD})}}{\pi}\frac{(1+e)^{1.1954}}{[a(1-e^2)]^{1.5}}. \tag{18}$$

The characteristic strain at the nth harmonic can be calculated as (Barack & Cutler 2004)

$$h_{c,n}^2=\frac{1}{(\pi D)^2}\left(\frac{2G}{c^3}\frac{\dot{E}_n}{\dot{f}_n}\right), \tag{19}$$

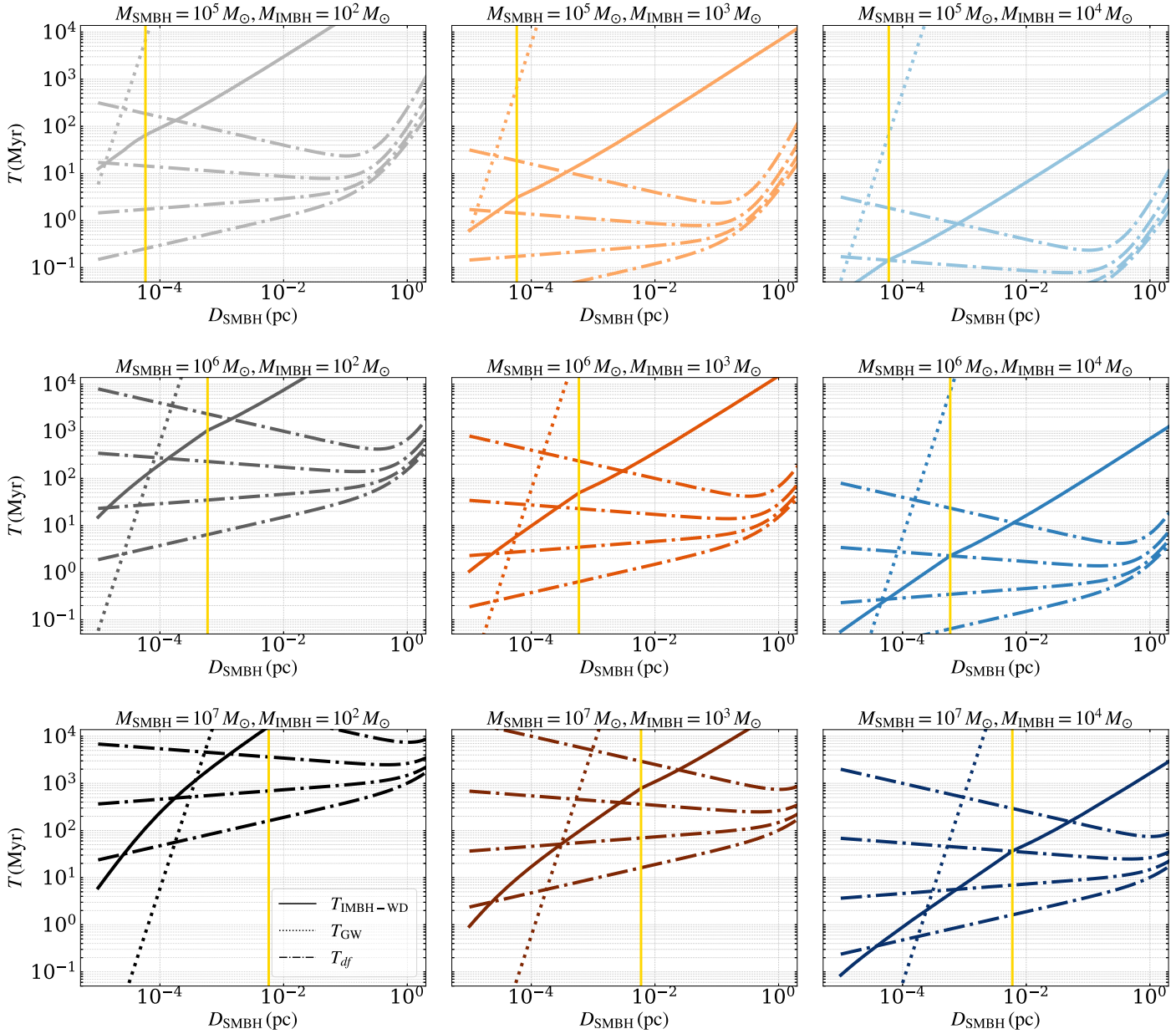

Figure 3. Comparison between timescales. In each panel, the solid curve shows the tidal capture/disruption timescale ($T_{\rm IMBH-WD}$; Equation (5)) at a given galactocentric distance. The vertical yellow line is the distance at which the maximum tidal capture radius is smaller than the tidal disruption radius. On the right side of the yellow line, the solid curve shows the tidal capture timescale, and on the left it shows the timescale of the tidal disruption events (TDEs). The dotted line shows the GW inspiral timescale of the IMBH toward the SMBH (Equation (15), assuming $e_{\rm IMBH} = 0$). The dotted–dashed curves indicate the dynamical friction timescales for stellar number density distributions with different slopes α. From top to bottom, $\alpha = 1.2$, 1.4, 1.6, and 1.8. The slope of the WD number density distribution is fixed to be 1.4 (Hopman & Alexander 2006) for the calculation of the tidal capture/disruption timescales. Tidal capture interactions or disruptions are possible when $T_{\rm IMBH-WD} < \min(T_{\rm df}, T_{\rm GW})$.

where D is the luminosity distance to the source, $\dot{f}_n$ is the time derivative of the GW frequency of the nth harmonic in the rest frame, and $\dot{E}_n$ is the GW power radiated at f_n. The frequency at the nth harmonic is given by the orbital frequency of the binary $f_n = nf_{\rm orb}$, and $f_{\rm orb} = \sqrt{GM_{\rm tot}/a^3}/2\pi$ where $M_{\rm tot}$ is the total mass of the binary. The radiated power $\dot{E}_n$ can be written as (Peters & Mathews 1963)

$$\dot{E}_n = \frac{32}{5}\frac{G^{7/3}}{c^5}(2\pi f_{\rm orb}\,\mathcal{M}_c)^{10/3} g(n, e), \tag{20}$$

where $\mathcal{M}_c$ is the chirp mass in the rest frame and $\mathcal{M}_c = (M_{\rm IMBH}M_{\rm WD})^{3/5}/M_{\rm tot}^{1/5}$. The time derivative of the frequency is computed to be

$$\dot{f}_n = n\frac{96}{10\pi}\frac{(G\mathcal{M}_c)^{5/3}}{c^5}(2\pi f_{\rm orb})^{11/3} F(e). \tag{21}$$

Knowing the characteristic strains and the GW frequencies, we can calculate the signal-to-noise ratio S/N for eccentric binaries by summing over the relevant harmonics:

$$({\rm S/N})^2 = \sum_{n=1}^{\infty}\int_{f_n}^{f'_n}\left[\frac{h_{c,n}}{h_f}\right]^2\frac{df_n}{f_n}, \tag{22}$$

where h_f is the LISA noise curve from Robson et al. (2019), and f'_n is the GW frequency of the nth harmonic at the end of

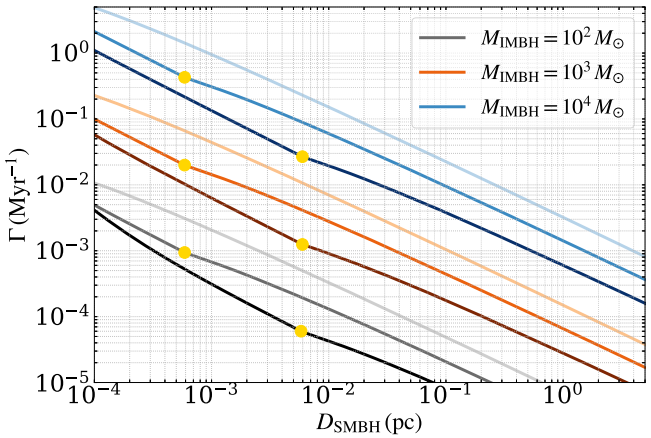

Figure 4. The rates of WDs captured or disrupted tidally by IMBHs in the galactic nuclei as a function of the galactocentric distances. Each curve shows the rate of one IMBH and the colors have the same meanings as in Figure 2. The yellow dot on each curve marks the turning point where the maximum tidal capture radius becomes smaller than the tidal disruption radius. If a yellow dot is missing then for the range of distances shown in the figure the tidal capture radius is always larger than the tidal disruption radius.

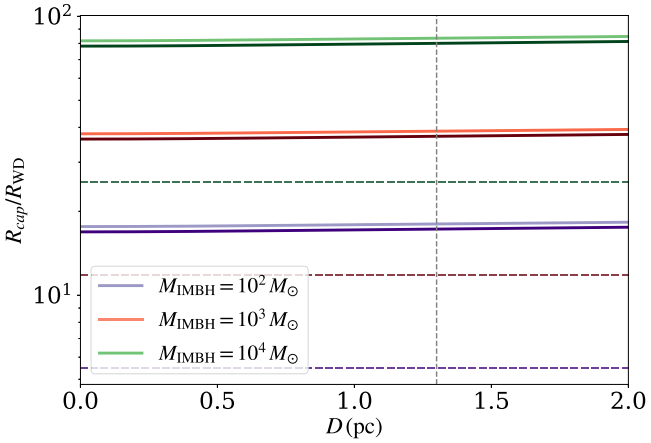

Figure 5. Similar to Figure 2, but for GCs. The three colors/groups of curves correspond to three IMBH masses of $10^4\ M_\odot$ (green), $10^3\ M_\odot$ (red), and $10^2\ M_\odot$ (purple) from top to bottom. For each group of curves, the top and bottom curves are for cluster masses of 2×10^5 and $5\times10^5\ M_\odot$, respectively. The vertical line shows the half-mass radius of the clusters where $b = 1$ pc (Equation (16)).

the LISA observation time. We truncate the calculation at the maximum harmonic (O'Leary et al. 2009)

$$n_{\rm max} = 5\frac{(1+e)^{0.5}}{(1-e)^{1.5}}, \tag{23}$$

which is about 7053 for $e = 0.99$. Here we did not consider the orbital decay from tidal effects because Vick et al. (2017) showed that they are negligible compared to GW radiation. The characteristic strains for binaries at 1 Mpc in comparison to the LISA sensitivity curve are shown as an example in Figure 7. Note that the characteristic strains are only accurate up to when tidal stripping starts since we assume no mass loss during the inspiral (Zalamea et al. 2010; see Section 4.2.2 for more details). The evolutionary time span of these strains (assuming inspiral stops at the tidal disruption radius) is about 390, 1830, and 8440 yr for $M_{\rm IMBH} = 10^4$, 10^3, and $10^2\,M_\odot$, respectively. Combining the duration of the GW signals with the capture

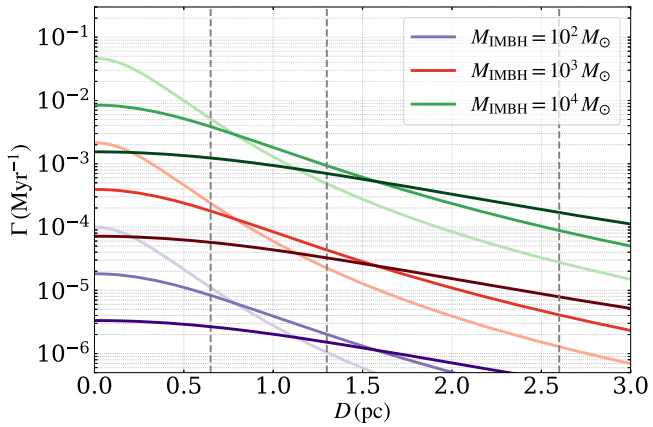

Figure 6. Similar to Figure 4, the rates of IMBH–WD tidal captures in GCs as a function of the distances to the cluster centers. Here we only show clusters with $M_{\rm cl} = 2\times10^5\ M_\odot$, and each cluster has one IMBH. Different colors are for different IMBH masses, and each group of curves with the same color but different shades shows the Plummer scale length $b = 0.5$, 1, and 2 pc from top to bottom. Smaller values of b indicate denser clusters. The three vertical lines are the half-mass radii for these three scale lengths.

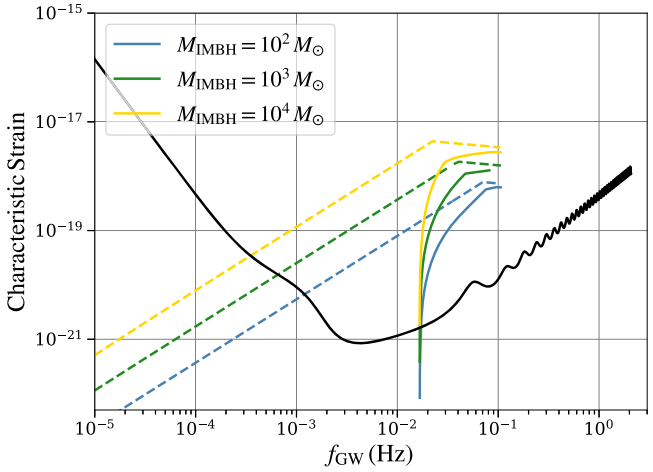

Figure 7. Evolution of the characteristic strain at the peak frequency of GW emission assuming a distance of 1 Mpc. The evolution has initial $a = 3R_t/(1-e)$ and $e = 0.99$, and stops at the commencement of the tidal disruption of the WD. We assume LISA has a four-year mission lifetime. The dashed curves indicate the inspirals of circular IMBH–WD binaries for comparison.

rates in Figures 4 and 6, we can expect $\sim10^{-4}$–10^{-3} events per Milky Way–like galaxy.

For S/N > 2, the GW signals can be detected out to about 73, 15, and 3 Mpc for $M_{\rm IMBH} = 10^4$, 10^3, and $10^2\,M_\odot$, respectively. If we require that S/N > 10, the maximum detectable distances are 14, 3, and 1 Mpc instead for the same three IMBH masses. These values are consistent with Sesana et al. (2008), which showed that the GW emission with S/N > 30 can be detected out to ≈200 Mpc for BHs with masses in the range $\approx10^4$–$10^5\,M_\odot$, WDs with masses in the range ≈0.5–1 $M_\odot$, and circular orbits at tidal disruption or the innermost stable orbit.

4.2. Electromagnetic Counterparts

As discussed above and illustrated in Figure 3, tidal capture dominates in GCs and at relatively larger distances in galactic nuclei, while in the innermost regions of the latter WDs are tidally disrupted more efficiently. The associated

electromagnetic counterparts are expected to be qualitatively and quantitatively different in the two situations, and hence we discuss them separately below.

4.2.1. Prompt Tidal Disruption (near Parabolic Orbit)

Prompt tidal disruption of a WD by an IMBH will occur if the WD passes sufficiently close to the IMBH such that the pericenter R_p of its orbit becomes smaller than the tidal disruption radius defined in Equation (7). The strength of the encounter is measured by the penetration factor

$$\beta \equiv \frac{R_t}{R_p} = \left(\frac{R_p}{R_{\rm WD}}\right)^{-1}\left(\frac{M_{\rm IMBH}}{M_{\rm WD}}\right)^{1/3}. \quad (24)$$

The outcome of the encounter will depend on the value of β (Rosswog et al. 2009). Let us first consider the more typical case of $\beta \gtrsim 1$, which has been well studied in the limit in which the debris has a uniform spread in energy between a minimum value (the most bound debris) and a maximum (unbound) (Rees 1988). Under these conditions, about half of the debris from the tidal disruption remains bound to the IMBH and falls back, while the other half is unbound. Accretion of the bound debris onto the IMBH begins on a timescale determined by the fallback of the most bound debris:

$$t_{\rm fb} \approx 2\pi\left(\frac{R_{\rm WD}^3 M_{\rm IMBH}}{GM_{\rm WD}^2}\right)^{1/2} \approx 10^3\ {\rm s} \times \left(\frac{M_{\rm IMBH}}{10^3\,M_\odot}\right)^{1/2}\left(\frac{M_{\rm WD}}{0.6\,M_\odot}\right)^{-1}\left(\frac{R_{\rm WD}}{10^4\ {\rm km}}\right)^{3/2}. \quad (25)$$

After an initial rapid rise, the late-time fallback rate (on timescales $\gg t_{\rm fb}$) of the tidally disrupted bound debris is expected to follow a power-law decay as

$$\dot{M}_{\rm fb}(t) \approx \dot{M}_{\rm fb}(t_{\rm fb})\left(\frac{t}{t_{\rm fb}}\right)^{-5/3}, \quad (26)$$

where the peak rate $\dot{M}_{\rm fb}(t_{\rm fb})$ is of the order of

$$\dot{M}_{\rm fb}(t_{\rm fb}) \approx \frac{M_{\rm WD}}{3t_{\rm fb}} \approx 2\times 10^{-4}\,M_\odot\ {\rm s}^{-1} \times \left(\frac{M_{\rm IMBH}}{10^3\,M_\odot}\right)^{-1/2}\left(\frac{M_{\rm WD}}{0.6\,M_\odot}\right)^{2}\left(\frac{R_{\rm WD}}{10^4\ {\rm km}}\right)^{-3/2}. \quad (27)$$

The precise fate of the fallback material can only be determined via numerical simulations. Whether the fallback material is able to circularize depends on its ability to lose a significant amount of energy. Hydrodynamic simulations by Kawana et al. (2018) show that WD–BH TDEs result in a variety of outcomes depending on the WD/BH masses and pericenter of the orbit. They find a subset of cases where self-interception of the stream occurs, favoring circularization of the debris and the onset of super-Eddington accretion rates. Strong outflows and relativistic jets are likely to ensue in these situations. The accretion rate onto the BH (and hence the emitted power) tracks the fallback rate as long as the viscous timescale of the disk is shorter than the fallback time. Assuming that a jet can be launched with efficiency ϵ_j and that a fraction ϵ_γ of the jet energy is dissipated into high-energy radiation, then transients with luminosities $\sim(10^{46}$–$10^{47})(\epsilon_j/0.1)(\epsilon_\gamma/0.1)$ erg s^{-1} can be expected.

When the WD approaches the IMBH with a large penetration factor, it can be severely compressed to the extent that explosive nuclear burning can be ignited (Luminet & Pichon 1989; Rosswog et al. 2009). During the period of compression, elements up to the iron group can be synthesized, which are then injected into the outflow with the explosion. The explosive transient would observationally manifest as a peculiar, underluminous thermonuclear explosion (Rosswog et al. 2008a). At the same time, a sizable fraction of the debris (∼35%, Rosswog et al. 2009) would still remain bound and accrete to the BH, possibly after circularization onto a disk.

There have already been several unusual transients for which the tidal disruption of a WD by an IMBH provides a compelling explanation. Krolik & Piran (2011) suggested this progenitor model for Swift J1644 + 57 (Burrows et al. 2011), a bright X-ray source (peak isotropic luminosity $\sim 4\times 10^{48}$ erg s^{-1}) which, after a steady period of about 700 s, underwent several flaring events separated by longer timescales. These were interpreted as the result of repeated close passages and hence stripping. Shcherbakov et al. (2013) suggested that the unusual pair of the gamma-ray burst (GRB) 060218 and the accompanying supernova SN 2006aj may be the result of a WD that is tidally disrupted by a BH of $\sim 10^4\ M_\odot$. The unusually long GRB, of about 2600 s duration and equivalent isotropic luminosity $\sim 10^{47}$ erg s^{-1} (Campana et al. 2006), is compatible with the typical accretion timescale expected in these events, while the unusual supernova, the fastest of all the ones associated with GRBs, could have been the result of tidal pinching and ignition of the WD. More generally, tidal disruption of a WD by an IMBH is considered a good alternative model (to massive star collapse) for the subset of ultralong GRBs (ULGRBs, Levan et al. 2014, 2016). The rates of these events are rather uncertain, but a rough estimate is placed at about 0.01 Myr^{-1} per galaxy (Gendre et al. 2013; Levan et al. 2016). Assuming (lacking direct observational data) that the rate of jetted TDEs from WDs disrupted by IMBHs is similar to that of the well studied events of stellar disruptions by SMBHs, and that is a few percent of events (van Velzen et al. 2016), then a rate of 0.1 Myr^{-1} as estimated in Section 3.1 for a typical case of a $10^3\ M_\odot$ IMBH and a $10^6\ M_\odot$ SMBH would imply a rate of ∼0.001 Myr^{-1} jetted events, hence making WD disruptions by IMBHs a potentially important channel of ULGRB progenitors (i.e., ∼10% with the estimates above).

Among transients of different nature, Peng et al. (2019) suggested that the tidal disruption of a WD by an IMBH is responsible for producing the two fast X-ray transients, CDF-S XT1 (Bauer et al. 2017) and XT2 (Xue et al. 2019, with a peak luminosity $\sim 3\times 10^{45}$ erg s^{-1}), characterized by an initial X-ray plateau lasting around hundreds to thousands of seconds, followed by a rapid decay in the light curve. Rates for these X-ray transients have been estimated to be in the range ∼1–10^3 Gpc^{-3} (depending on the redshift) from CDF-S XT1 (Bauer et al. 2017) and $\sim 10^4$ Gpc^{-3} from CDF-S XT2 (Xue et al. 2019). Assuming a galaxy density of 10^8 Gpc^{-3} (Conselice et al. 2016), these estimates would yield an event rate per galaxy for these transients in the range 10^{-2}–10^2 Myr^{-1}. Since their X-ray emission has been modeled directly as the result of accretion (i.e., no jet requirement), our estimated disruption rates of 0.1 Myr^{-1} would give plausibility to this interpretation for at least a fraction of transients. Most recently, Gomez & Gezari (2023) has shown that

SN 2020lrt may be a candidate for a WD being tidally compressed and disrupted by an IMBH.

4.2.2. Tidal Stripping after Tidal Capture (Eccentric Orbit)

Once the WD has been captured by the IMBH, the orbit of the newly formed IMBH–WD binary will begin to shrink due to GW emission, as discussed in Section 4.1.

Mass loss in interacting binaries with eccentric orbits was studied by Sepinsky et al. (2007). They showed that stripping of the outer layers of the WD begins when the pericenter of the orbit becomes small enough that the radius of the WD exceeds its Roche lobe, that is

$$R_{\rm WD} \gtrsim R_{\rm lobe} \approx \gamma R_p \left(\frac{M_{\rm IMBH}}{M_{\rm WD}}\right)^{-1/3}, \quad (28)$$

where the parameter γ in the expression for the Roche lobe depends on the orbital eccentricity, the mass ratio of the two objects in the binary, and the rotation of the WD. An average value is taken to be $\gamma \approx 0.5$. As the WD makes repeated passages through the pericenter of its orbit, mass gets stripped. This process was first studied semianalytically by Zalamea et al. (2010), and subsequently, with an increasing degree of sophistication, by MacLeod et al. (2014), Vick et al. (2017), and Chen et al. (2023). The qualitative features of the phenomenon are similar in all these works, while quantitative details vary depending on the various approximations made. Here, we will follow the more recent Chen et al. (2023), who compared their analytical formalism against hydrodynamic simulations. For a penetration factor $\beta \lesssim 0.7$, they found that the fraction of mass lost, $\Delta M/M_{\rm WD}$, at each pericenter passage can be well approximated (when compared to numerical results) by the expression

$$\frac{\Delta M}{M_{\rm WD}} \simeq 4.8\left[1-\left(\frac{M_{\rm WD}}{M_{\rm Ch}}\right)^{4/3}\right]^{3/4}\left(1-\frac{\gamma}{\beta}\right)^{5/2}, \quad (29)$$

where $M_{\rm Ch} = 1.4\ M_\odot$ is the Chandrasekhar mass. The stripped debris is found to remain bound to the IMBH for eccentricities below a critical value

$$e_{\rm crit} \lesssim 1 - 0.078\ \xi\ \beta\ M_{\rm IMBH}^{-1/3}\left(\frac{M_{\rm WD}}{0.6\ M_\odot}\right)^{1/3}, \quad (30)$$

where the parameter ξ quantifies the uncertain tidal effects. From numerical simulations, they found $e_{\rm crit} \sim 0.8$–0.9 for a WD of 0.67 $M_\odot$, and $e_{\rm crit} \sim 0.7$–0.8 for a WD of 1.07 $M_\odot$.

Figure 8 shows the distribution of eccentricities at capture (upper panel and solid lines), as well as at the moment when tidal stripping begins[7] (bottom panel—note that the condition in Equation (28) with $\gamma \approx 0.5$ is equivalent to $R_p \lesssim 2R_t$). While the eccentricity is close to one at capture, for systems that are captured with $R_p > 2R_t$, the eccentricity drops quickly by the time mass loss begins. Except for the narrow range of capture parameters $[2R_p/R_t$–$2.2R_p/R_t]$, the eccentricity is below the critical value in Equation (30), and hence the stripped mass is expected to remain fully bound.

[7] Note that, if at the time that mass stripping starts the WD is rather found in a circular orbit, then the following evolution is characterized by stable mass transfer, which, depending on the conditions, may lead to the WD receding from the IMBH while filling its Roche lobe (Dai & Blandford 2013).

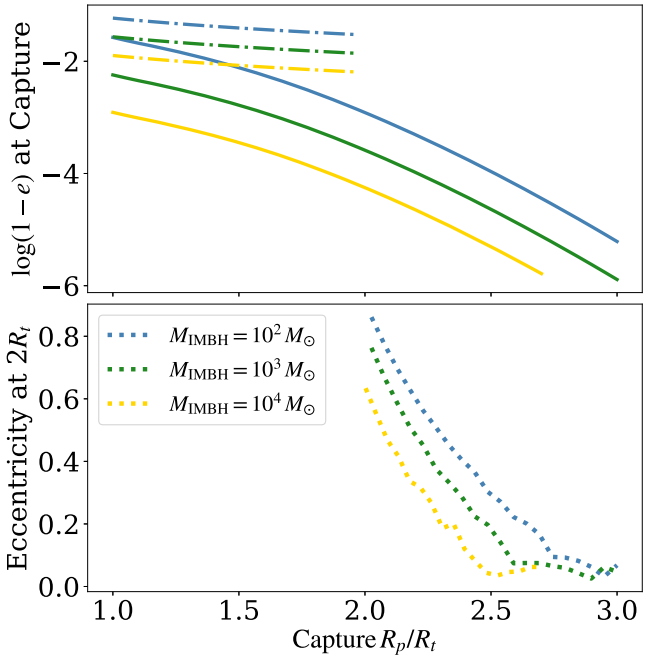

Figure 8. Eccentricity distributions of the WDs at the moment of capture (upper panel, solid curves) and at the moment of initial mass loss after some degrees of inspiral (when $R_p \sim 2R_t$, bottom panel). Also plotted in the upper panel are the critical eccentricities for the stripped mass to remain bound to the IMBHs from Equation (30) assuming $\xi = 3.5$ (Chen et al. 2023; dotted–dashed curves). The x-axis shows the pericenter distance at capture. The colors of the curves distinguish different IMBH masses.

Once mass loss has begun, the subsequent mass loss rate undergoes two phases. At early times, the mass loss follows the orbital shrinkage driven by the emission of GW radiation. Later, as the smaller WD expands and becomes less dense, it becomes easier to disrupt after each passage, until it is completely disrupted after a time $t_{\rm ML}$. Chen et al. (2023) showed that this timescale is generally shorter than the GW timescale by a factor

$$\frac{t_{\rm ML}}{t_{\rm GW}} \simeq 0.02\left(\frac{M_{\rm IMBH}}{10^4\ M_\odot}\right)^{4/15}\left(\frac{M_{\rm WD}}{0.6\ M_\odot}\right)^{16/15}\left(\frac{1-e_0}{0.1}\right)^{-1}, \quad (31)$$

where e_0 is the eccentricity at the beginning of the mass loss.

At the same time, mass loss will proceed with modulation on the binary period and increasing amplitude as the WD gets increasingly more stripped (Zalamea et al. 2010; MacLeod et al. 2014). The fallback rate of the tidally disrupted debris is also expected to display such a modulation, as long as the accretion timescale is shorter than the orbital period P. The calculations by Chen et al. (2023) showed that a good approximation to the results of their numerical simulations for the ratio between these two timescales is

$$\frac{t_{\rm fb}}{P} \simeq \left[1+\frac{2\xi\beta}{1-e}\left(\frac{M_{\rm IMBH}}{M_{\rm WD}}\right)^{-1/3}\right]^{-3/2}. \quad (32)$$

For the range of parameters β (0.55–0.7), orbital parameters ($0.7 \leqslant e \leqslant 0.9$), and WD masses (0.67 and 1.67 $M_\odot$) explored in their simulations, they found the above timescale ratio to be ∼0.2–0.5. The average fallback rate over an orbital period can be estimated as $\dot{M}_{\rm fb} \sim \Delta M/P$ (since, as discussed above, the greatest majority of our systems are found to be in a regime where all the stripped mass remains bound). For typical orbital

parameters, its peak magnitude is found to exceed the Eddington value by several orders of magnitude, that is $\dot{M}_{\rm fb} \sim 10^{-5}$--$10^{-3}\,M_\odot\,{\rm s}^{-1}$ (Zalamea et al. 2010; MacLeod et al. 2014; Chen et al. 2023). The modulation of the accretion rate onto the IMBH will further depend on the accretion (viscous) timescale if disk circularization occurs. The ratio between the accretion timescale and the orbital period can be estimated as (e.g., MacLeod et al. 2014)

$$\frac{t_{\rm acc}}{P} \simeq 0.2\left(\frac{1-e}{0.03}\right)^{3/2}\left(\frac{\alpha}{0.1}\right)^{-1}\left(\frac{H/R}{0.5}\right)^{-2}, \quad (33)$$

in a viscously accreting ring of scale height H with viscosity parameter α (Shakura & Sunyaev 1973). Given the range of $\alpha \sim 0.01$–0.1, these timescales can be comparable. Modulation in the accretion rate onto the IMBH will still be expected even when partially smoothed out by viscosity.

Detailed predictions of the luminosity and its spectrum during the periodic mass-loss phase are still lacking, since they depend heavily on whether an outflow and/or a jet can be driven. If the electromagnetic emission is the direct result of accretion onto the IMBH, then it will be Eddington-limited, and hence, for the IMBH masses considered here, luminosities would be limited to the range 10^{40}–10^{42} erg s^{-1}. However, considering that the accretion rates are highly super-Eddington, it is plausible that outflows and jets could be driven, in analogy to the standard TDE case discussed in the previous subsection. If a fraction ϵ $(=\epsilon_j\epsilon_\gamma)$ of accreted mass is converted to luminosity, the peak fallback rates reported above would lead to an emission $L = \epsilon \dot{M}_{\rm fb} c^2 \sim (\epsilon/0.01)(10^{45}$–$10^{47})$ erg s^{-1}. The luminosity would vary with the binary period and last for a timescale $\sim t_{\rm ML}$.[8]

Tidal stripping of a WD by an IMBH in a binary has already been invoked to explain some unusual, rare transients. Shen (2019) suggested this progenitor system as a potential progenitor candidate for the ultraluminous X-ray flares, with rapid rise (∼minute) and decay (∼hour) and peak luminosities $\sim 10^{40}$–10^{41} erg s^{-1}, that are observed in GCs and elliptical galaxies (Irwin et al. 2016; see also Karpiuk et al. 2022 for modeling of these sources). Similarly, King (2020) proposed the WD tidal stripping model to explain the quasi-periodic ultrasoft X-ray eruptions (with durations of 10^3--10^4 s, periods of about 9 hr, and peak luminosity $\sim 5 \times 10^{42}$ erg s^{-1}) observed from the galaxy GSN 069 (Miniutti et al. 2019). Sources of this brightness have been resolved by the Chandra telescope up to redshifts ∼4 (Wilkes 2019), and will be detectable up to $\gtrsim$300 Mpc with a short ∼10 s exposure time by the Follow-up X-ray Telescope of the upcoming mission Einstein Probe (Yuan et al. 2015).

5. Conclusions and Discussion

In this study, we estimated the rates of WDs tidally captured by IMBHs in dense stellar environments. We assumed that a typical WD behaves as an $n = 1.5$ polytrope and computed the capture radii based on the energy dissipated through WD oscillations during the first passage of the IMBH–WD encounter. We computed the capture rates for IMBHs with various masses in two environments, galactic nuclei and GCs. For the galactic nuclei, we adopted power-law distributions of stars and WDs around the central SMBHs, and studied how different SMBH masses and slopes of the stellar distribution affect the capture rates. We adopted Plummer profiles with different masses and half-mass radii in the case of GCs. Using these analytical models, we demonstrated that for a Milky Way–like galactic nucleus, the capture rate is ∼0.02 per Myr for an IMBH of $10^3\,M_\odot$. Meanwhile, the capture rate is about a few times 0.1 per Myr in a Milky Way–like galaxy if we assume that all GCs contain an IMBH.

These captured IMBH–WD binaries are sources of intermediate-mass-ratio inspirals and radiate GWs in the LISA frequency band. We calculated the characteristic strains and S/N for inspiralling eccentric IMBH–WD binaries and showed that their GW signals may be detected out to ∼100 Mpc by LISA. Following the phase of GW radiation, which shrinks the orbits of the IMBH–WD binaries, tidal stripping and disruption of the WDs by the IMBHs will take effect. The luminosity of the electromagnetic emission during the periodic mass loss is at least $\gtrsim 10^{40}$–10^{42} erg s^{-1} (depending on the IMBH mass, if Eddington-limited). If aided by the launch of an outflow or jet, the luminosity may reach $\sim 10^{45}$–10^{47} erg s^{-1}, comparable to that of standard TDEs (MacLeod et al. 2014).

The capture and disruption rates and gravitational S/N estimated here should be taken as upper limits. We assumed that energy deposited into the WDs is efficiently dissipated, and the structure of the WDs stays unchanged during capture and inspiral. This essentially neglects any buildup of oscillation energy in the WDs and the possibility of WD disruption, allowing for all WDs that approach close to an IMBH to be captured into a lasting binary. For example, during very close approaches ($R_p \lesssim 2R_t$), the degeneracy of the WD's outermost layer may be lifted by shock heating, leading to faster mass loss (e.g., Cheng & Evans 2013). We also did not consider WD spins, which could play an important role in the orbital evolution of the binaries (e.g., Ivanov & Papaloizou 2007; Vick et al. 2017). These are reasonable assumptions for the first-order rate approximation here. A more detailed understanding of the WDs' reaction to the strong tidal force will require numerical calculations. For the computation of the GW emission, we followed the WD until its pericenter reaches the tidal disruption radius. However, both the magnitude of the signal and its duration should be considered as upper limits since tidal stripping reduces the WD mass and shortens the inspiral time. In addition, the IMBH occupation fraction and the mass distribution in galactic nuclei and in GCs are uncertain. Larger occupation fractions and flatter mass distributions will lead to higher tidal capture rates and vice versa. Future (non)detection of IMBH–WD inspirals and electromagnetic emissions would be able to shed more light on the existence of IMBHs and potentially supply data for probing this wide range of physics.

[8] Note that this timescale does not account for the modifications to the WD structure where the outer layer of the WD is expected to heat up and ignite before the point of disruption due to tidal heating (Vick et al. 2017).

Acknowledgments

We thank Fred Rasio, Kyle Kremer, Chris Matzner, and the anonymous referee for helpful discussions and comments. This work was supported by NSF Grant AST-2108624 at Northwestern University, and by the Natural Sciences and Engineering Research Council of Canada (NSERC) DIS-2022-568580. G.F. acknowledges support from NASA Grant 80NSSC21K1722. R.P. acknowledges support by NSF award AST-2006839. This research was supported in part through the computational resources and staff contributions provided for

the Quest high performance computing facility at Northwestern University, which is jointly supported by the Office of the Provost, the Office for Research, and Northwestern University Information Technology.

ORCID iDs

Claire S. Ye https://orcid.org/0000-0001-9582-881X
Giacomo Fragione https://orcid.org/0000-0002-7330-027X
Rosalba Perna https://orcid.org/0000-0002-3635-5677

References

Abbott, R., Abbott, T. D., Abraham, S., et al. 2020, PhRvL, 125, 101102
Amaro-Seoane, P., Audley, H., Babak, S., et al. 2017, arXiv:1702.00786
Amaro-Seoane, P., Gair, J. R., Freitag, M., et al. 2007, CQGra, 24, R113
Anninos, P., Fragile, P. C., Olivier, S. S., et al. 2018, ApJ, 865, 3
Antonini, F., Gieles, M., & Gualandris, A. 2019, MNRAS, 486, 5008
Barack, L., & Cutler, C. 2004, PhRvD, 69, 082005
Bauer, F. E., Treister, E., Schawinski, K., et al. 2017, MNRAS, 467, 4841
Baumgardt, H., Amaro-Seoane, P., & Schödel, R. 2018, A&A, 609, A28
Baumgardt, H., Makino, J., & Ebisuzaki, T. 2004, ApJ, 613, 1143
Binney, J., & Tremaine, S. 2008, Galactic Dynamics: Second Edition (Princeton, NJ: Prinston Univ. Press)
Burrows, D. N., Kennea, J. A., Ghisellini, G., et al. 2011, Natur, 476, 421
Campana, S., Mangano, V., Blustin, A. J., et al. 2006, Natur, 442, 1008
Chen, J.-H., Shen, R.-F., & Liu, S.-F. 2023, ApJ, 947, 32
Cheng, R. M., & Evans, C. R. 2013, PhRvD, 87, 104010
Clausen, D., & Eracleous, M. 2011, ApJ, 726, 34
Conselice, C. J., Wilkinson, A., Duncan, K., & Mortlock, A. 2016, ApJ, 830, 83
Dai, L., & Blandford, R. 2013, MNRAS, 434, 2948
Fabian, A. C., Pringle, J. E., & Rees, M. J. 1975, MNRAS, 172, 15
Fragione, G., Ginsburg, I., & Kocsis, B. 2018a, ApJ, 856, 92
Fragione, G., Kocsis, B., Rasio, F. A., & Silk, J. 2022, ApJ, 927, 231
Fragione, G., & Leigh, N. 2018, MNRAS, 480, 5160
Fragione, G., Leigh, N. W. C., Ginsburg, I., & Kocsis, B. 2018b, ApJ, 867, 119
Fragione, G., & Loeb, A. 2023, ApJ, 944, 81
Gallego-Cano, E., Schödel, R., Dong, H., et al. 2018, A&A, 609, A26
Gallego-Cano, E., Schödel, R., Nogueras-Lara, F., et al. 2020, A&A, 634, A71
Gendre, B., Stratta, G., Atteia, J. L., et al. 2013, ApJ, 766, 30
Giersz, M., Leigh, N., Hypki, A., Lützgendorf, N., & Askar, A. 2015, MNRAS, 454, 3150
Gomez, S., & Gezari, S. 2023, arXiv:2302.14070
Gondán, L., Kocsis, B., Raffai, P., & Frei, Z. 2018, ApJ, 860, 5
González, E., Kremer, K., Chatterjee, S., et al. 2021, ApJL, 908, L29
González Prieto, E., Kremer, K., Fragione, G., et al. 2022, ApJ, 940, 131
Greene, J. E., Strader, J., & Ho, L. C. 2020, ARA&A, 58, 257
Gürkan, M. A., Freitag, M., & Rasio, F. A. 2004, ApJ, 604, 632
Gürkan, M. A., & Rasio, F. A. 2005, ApJ, 628, 236
Haas, R., Shcherbakov, R. V., Bode, T., & Laguna, P. 2012, ApJ, 749, 117
Hills, J. G. 1988, Natur, 331, 687
Hopman, C., & Alexander, T. 2006, ApJL, 645, L133
Hurley, J. R., Pols, O. R., & Tout, C. A. 2000, MNRAS, 315, 543
Irwin, J. A., Maksym, W. P., Sivakoff, G. R., et al. 2016, Natur, 538, 356
Ivanov, P. B., & Papaloizou, J. C. B. 2007, A&A, 476, 121
Jani, K., Shoemaker, D., & Cutler, C. 2020, NatAs, 4, 260
Karpiuk, T., Nikołajuk, M., Ducci, L., & Brewczyk, M. 2022, arXiv:2208.11525
Kawana, K., Tanikawa, A., & Yoshida, N. 2018, MNRAS, 477, 3449
King, A. 2020, MNRAS Lett., 493, L120
Kremer, K., Spera, M., Becker, D., et al. 2020, ApJ, 903, 45
Krolik, J. H., & Piran, T. 2011, ApJ, 743, 134
Kroupa, P. 2001, MNRAS, 322, 231
Lee, H. M., & Ostriker, J. P. 1986, ApJ, 310, 176
Levan, A., Crowther, P., de Grijs, R., et al. 2016, SSRv, 202, 33
Levan, A. J., Tanvir, N. R., Starling, R. L. C., et al. 2014, ApJ, 781, 13
Luminet, J. P., & Pichon, B. 1989, A&A, 209, 103
MacLeod, M., Goldstein, J., Ramirez-Ruiz, E., Guillochon, J., & Samsing, J. 2014, ApJ, 794, 9
MacLeod, M., Guillochon, J., Ramirez-Ruiz, E., Kasen, D., & Rosswog, S. 2016a, ApJ, 819, 3
MacLeod, M., Trenti, M., & Ramirez-Ruiz, E. 2016b, ApJ, 819, 70
Maguire, K., Eracleous, M., Jonker, P. G., MacLeod, M., & Rosswog, S. 2020, SSRv, 216, 39
Mapelli, M., Bouffanais, Y., Santoliquido, F., Arca Sedda, M., et al. 2022, MNRAS, 511, 5797
McMillan, S. L. W., & Portegies Zwart, S. F. 2003, ApJ, 596, 314
Merritt, D. 2013, Dynamics and Evolution of Galactic Nuclei (Princeton, NJ: Princeton Univ. Press)
Miller, M. C. 2002, ApJ, 581, 438
Miller, M. C., & Hamilton, D. P. 2002, MNRAS, 330, 232
Miniutti, G., Saxton, R. D., Giustini, M., et al. 2019, Natur, 573, 381
O'Leary, R. M., Kocsis, B., & Loeb, A. 2009, MNRAS, 395, 2127
Peng, Z.-K., Yang, Y.-S., Shen, R.-F., et al. 2019, ApJL, 884, L34
Peters, P. C. 1964, PhRv, 136, 1224
Peters, P. C., & Mathews, J. 1963, PhRv, 131, 435
Plummer, H. C. 1911, MNRAS, 71, 460
Portegies Zwart, S. F., & McMillan, S. L. W. 2002, ApJ, 576, 899
Press, W. H., & Teukolsky, S. A. 1977, ApJ, 213, 183
Quinlan, G. D., & Shapiro, S. L. 1987, ApJ, 321, 199
Rees, M. J. 1988, Natur, 333, 523
Robson, T., Cornish, N. J., & Liu, C. 2019, CQGra, 36, 105011
Rosswog, S., Ramirez-Ruiz, E., & Hix, W. R. 2008a, ApJ, 679, 1385
Rosswog, S., Ramirez-Ruiz, E., & Hix, W. R. 2009, ApJ, 695, 404
Rosswog, S., Ramirez-Ruiz, E., Hix, W. R., & Dan, M. 2008b, CoPhC, 179, 184
Schödel, R., Gallego-Cano, E., Dong, H., et al. 2018, A&A, 609, A27
Sepinsky, J. F., Willems, B., & Kalogera, V. 2007, ApJ, 660, 1624
Sesana, A., Vecchio, A., Eracleous, M., & Sigurdsson, S. 2008, MNRAS, 391, 718
Shakura, N. I., & Sunyaev, R. A. 1973, A&A, 24, 337
Shapiro, S. L., & Teukolsky, S. A. 1983, Black Holes, White Dwarfs, and Neutron Stars: the Physics of Compact Objects (New York: Wiley)
Shcherbakov, R. V., Pe'er, A., Reynolds, C. S., et al. 2013, ApJ, 769, 85
Shen, R.-F. 2019, ApJL, 871, L17
Šubr, L., Fragione, G., & Dabringhausen, J. 2019, MNRAS, 484, 2974
Tanikawa, A., Giersz, M., & Arca Sedda, M. 2022, MNRAS, 515, 4038
Tanikawa, A., Sato, Y., Nomoto, K., et al. 2017, ApJ, 839, 81
Toscani, M., Rossi, E. M., & Lodato, G. 2020, MNRAS, 498, 507
Tremaine, S., Gebhardt, K., Bender, R., et al. 2002, ApJ, 574, 740
van Velzen, S., Anderson, G. E., Stone, N. C., et al. 2016, Sci, 351, 62
Vick, M., Lai, D., & Fuller, J. 2017, MNRAS, 468, 2296
Wen, L. 2003, ApJ, 598, 419
Wilkes, B. J. 2019, A&G, 60, 6
Xue, Y. Q., Zheng, X. C., Li, Y., et al. 2019, Natur, 568, 198
Yuan, W., Zhang, C., Feng, H., et al. 2015, arXiv:1506.07735
Zalamea, I., Menou, K., & Beloborodov, A. M. 2010, MNRAS Lett., 409, L25